

# Adversarial Ensemble Training by Jointly Learning Label Dependencies and Member Models

Lele Wang<sup>1\*</sup> and Bin Liu<sup>2\*\*</sup>

<sup>1</sup> Research Center for Data Mining and Knowledge Discovery, Zhejiang Lab, Hangzhou, 311121 China

<sup>2</sup> Research Center for Applied Mathematics and Machine Intelligence, Zhejiang Lab, Hangzhou, 311121 China  
{wangll,liubin}@zhejianglab.com

**Abstract** Training an ensemble of diverse sub-models has been empirically demonstrated as an effective strategy for improving the adversarial robustness of deep neural networks. However, current ensemble training methods for image recognition typically encode image labels using one-hot vectors, which overlook dependency relationships between the labels. In this paper, we propose a novel adversarial ensemble training approach that jointly learns the label dependencies and member models. Our approach adaptively exploits the learned label dependencies to promote diversity among the member models. We evaluate our approach on widely used datasets including MNIST, FashionMNIST, and CIFAR-10, and show that it achieves superior robustness against black-box attacks compared to state-of-the-art methods. Our code is available at <https://github.com/ZJLAB-AMMI/LSD>.

**Keywords:** deep learning · model ensemble · adversarial attack · label dependency

## 1 Introduction

Deep neural networks (DNNs), also known as deep learning, have achieved remarkable success across many tasks in computer vision [1,2,3,4], speech recognition [5,6], and natural language processing [7,8]. However, numerous works have shown that modern DNNs are vulnerable to adversarial attacks [9,10,11,12,13,14]. Even slight perturbations to input images, which are imperceptible to humans, can fool a high-performing DNN into making incorrect predictions. Additionally, adversarial attacks designed for one model may deceive other models, resulting in wrong predictions - this issue is known as adversarial transferability

---

\* work done when he was with Research Center for Applied Mathematics and Machine Intelligence, Zhejiang Lab.

\*\* Correspondence author. This paper was accepted by 19th Inter. Conf. on Intelligent Computing (ICIC 2023).

[15,16,17,18]. These adversarial vulnerability issues pose significant challenges for real-life applications of DNNs, particularly for safety-critical problems such as self-driving cars [19,20]. As a result, there has been increasing attention on promoting robustness against adversarial attacks for DNNs.

Ensembling models has been shown to be a highly effective approach for improving the adversarial robustness of deep learning systems. The basic idea behind model ensembling is illustrated through a Venn diagram in Fig.1 [21]. The rectangle represents the space spanned by all possible orthogonal perturbations to an input instance, while the circle represents the subspace spanned by perturbations that are adversarial to the associated model. The shaded region represents the perturbation subspace that is adversarial to the model ensemble. In the case of a single model as shown in Fig.1(a), any perturbation within the circle results in misclassification of the input image. However, for cases that employ an ensemble of two or more models (Fig.1(b) and (c)), successful adversarial attacks require perturbations only within the shaded region, meaning that the attack must fool all individual models in the ensemble. Therefore, promoting diversity among individual models is an intuitive strategy to improve the adversarial robustness of a model ensemble as the less overlap there is among their corresponding adversarial subspaces, the greater the diversity of the individual models. The amount of overlap determines the dimensionality of the adversarial sub-space [21]. Throughout this paper, we use the terms individual model, sub-model, and member model interchangeably.

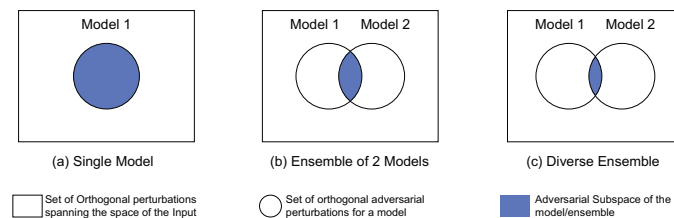


**Figure 1.** A conceptual illustration of the idea of using model ensembling to promote adversarial robustness: (a) single model; (b) an ensemble of two models; (c) an ensemble of two more diversified models. The shaded region denotes a subspace, adversarial attacks within which can fool the (ensemble) model to make a wrong prediction. This figure is drawn referring to Fig.1 of [21].

One challenge in applying model ensembling is how to promote diversity among member models while maintaining their prediction accuracy, particularly for non-adversarial inputs. The question becomes: how can we balance the trade-off between diversity and prediction quality during ensemble training? To address this issue, several advanced methods have been proposed in the literature [22,21,23,24,25]. For example, Pang et al. propose a diversity regularized cost function that encourages diversity in the non-maximal class predictions given by the last soft-max layers of the member models [22]. Kariyappa & Qureshi select

an ensemble of gradient misaligned models by minimizing their pairwise gradient similarities [21]. Yang et al. find that merely encouraging misalignment between pairwise gradients is insufficient to reduce adversarial transferability [25], and thus propose promoting both gradient misalignment and model smoothness. Sen et al. propose training an ensemble of models with different numerical precisions, where models with higher numerical precisions aim for prediction accuracy, while those with lower numerical precisions target adversarial robustness [23].

As previously mentioned, to apply state-of-the-art (SOTA) ensemble training methods, one must select a diversity metric to measure the diversity of member models. This metric may be the difference in non-maximal predictions given by the last soft-max layers of the member models [22], or the difference in gradient vectors associated with the member models [21]. It is worth noting that all these training methods use one-hot vectors to encode image classes, meaning each image in the training set is assigned a hard label. However, such hard labels cannot reflect any possible dependency relationships among image classes. Given an image, it is likely that dependency relationships exist between its associated classes. For example, in a handwritten digit image dataset, the number “0” may look more similar to “9” than to “4”; “3” may look more similar to “8” than to “7”, and so on. Conditional on a noisy input image, e.g., one whose ground truth label is “0”, there should exist a dependency relationship between labels “0” and “9”. Using hard labels omits such conditional dependency relationships.

Motivated by the above observation, we propose a novel ensemble training approach called Conditional Label Dependency Learning (CLDL) assisted ensemble training. Our approach jointly learns the conditional dependencies among image classes and member models. Compared to existing methods, our approach selects a different diversity metric that considers the difference in pairwise gradient vectors and predicted soft labels given by member models. The learned soft labels encode dependency relationships among the original hard labels. We find that our approach is more robust against black-box attacks compared to several state-of-the-art methods. In summary, the main contributions of this work are:

- We propose a novel diversity metric for adversarial ensemble training that incorporates information from both the gradient vectors associated with member models and predicted soft labels given by member models.
- We adapt a label confusion learning (LCL) model developed in [26] to generate soft labels of images in the context of adversarial ensemble training, originally used for enhancing text classification..
- We propose a CLDL-assisted ensemble training algorithm and demonstrate that it complements existing ensemble training methods. In particular, we show that our algorithm is more robust against black-box attacks compared to several state-of-the-art methods.

The remainder of this paper is organized as follows. In Section 2, we present some preliminary information. In Section 3, we describe our CLDL-based ensemble training method in detail. In Section 4, we present the experimental results. We conclude the paper in Section 5.

## 2 Preliminary

In this section, we present the preliminary knowledge that is related to our work.

### 2.1 Notations

Here we consider a DNN based image recognition task, which involves  $C$  classes. Following [25], let  $\mathcal{X}$  denote the input space of the DNN model,  $\mathcal{Y} = \{1, 2, \dots, C\}$  the class space. A DNN model is trained to yield a mapping function  $\mathcal{F} : \mathcal{X} \rightarrow \mathcal{Y}$ . Let  $x$  denote a clean image and  $x'$  an adversarial counterpart of  $x$ . Let  $\epsilon$  be a pre-set attack radius that defines the maximal magnitude of an adversarial perturbation. That says, for any adversarial perturbation, its  $L_p$  norm is required to be less than  $\epsilon$ . Let  $\ell_{\mathcal{F}}(x, y)$  denote the cost function used for training the model  $\mathcal{F}(x, \theta)$ , where  $\theta$  denotes the parameter of the model.

### 2.2 Definitions

**Definition 1 Adversarial attack**[25]. *Given an input  $x \in \mathcal{X}$  with true label  $y \in \mathcal{Y}$ ,  $F(x) = y$ . (1) An untargeted attack crafts  $\mathcal{A}_U(x) = x + \delta$  to maximize  $\ell_{\mathcal{F}}(x + \delta, y)$  where  $\|\delta\|_p \leq \epsilon$ . (2) A targeted attack with target label  $y_t \in \mathcal{Y}$  crafts  $\mathcal{A}_T(x) = x + \delta$  to minimize  $\ell_{\mathcal{F}}(x + \delta, y_t)$  where  $\|\delta\|_p \leq \epsilon$  and  $\epsilon$  is a pre-defined attack radius that limits the power of the attacker.*

**Definition 2 Alignment of loss gradients**[25,21]. *The alignment of loss gradients between two differentiable loss functions  $\ell_{\mathcal{F}}$  and  $\ell_{\mathcal{G}}$  is defined as:*

$$CS(\nabla_x \ell_{\mathcal{F}}, \nabla_x \ell_{\mathcal{G}}) = \frac{\nabla_x \ell_{\mathcal{F}}(x, y) \cdot \nabla_x \ell_{\mathcal{G}}(x, y)}{\|\nabla_x \ell_{\mathcal{F}}(x, y)\|_2 \cdot \|\nabla_x \ell_{\mathcal{G}}(x, y)\|_2} \quad (1)$$

*which is the cosine similarity between the gradients of the two loss functions for an input  $x$  drawn from  $\mathcal{X}$  with any label  $y \in \mathcal{Y}$ . If the cosine similarity of two gradients is -1, we say that they are completely misaligned.*

### 2.3 Adversarial Attacks

Adversarial attacks aim to create human-imperceptible adversarial inputs that can fool a high-performing DNN into making incorrect predictions. These attacks are typically divided into two basic classes: white-box attacks, which assume the adversary has full knowledge of the model’s structures and parameters, and black-box attacks, which assume the adversary has no access or knowledge of any information regarding the model. Here we briefly introduce four typical white-box attacks involved in our experiments while referring readers to review papers [27,28,29] and references therein for more information on adversarial attacks.

**Fast Gradient Sign Method (FGSM)** FGSM is a typical white-box attacking method to find adversarial examples. It performs a one-step update along

the direction of the gradient of the adversarial loss. Specifically, it generates an adversarial example  $x'$  by solving a maximization problem as follows [9]:

$$x' = x + \varepsilon \cdot \text{sign}(\nabla_x \ell(x, y)), \quad (2)$$

where  $\varepsilon$  denotes the magnitude of the perturbation,  $x$  the original benign image sample,  $y$  the target label of  $x$ , and  $\nabla_x \ell(x, y)$  the gradient of the loss  $\ell(x, y)$  with respect to  $x$ .

**Basic Iterative Method (BIM)** BIM is an extension of FGSM, which performs FGSM iteratively to generate an adversarial example as follows [30]:

$$x'_i = \text{clip}_{x, \varepsilon} \left( x'_{i-1} + \frac{\varepsilon}{r} \cdot \text{sign}(g_{i-1}) \right) \quad (3)$$

where  $x'_0 \triangleq x$ ,  $r$  is the number of iterations,  $\text{clip}_{x, \varepsilon}(A)$  is a clipping function that projects  $A$  in a  $\varepsilon$ -neighbourhood of  $x$ , and  $g_i \triangleq \nabla_x \ell(x'_i, y)$ .

**Projected Gradient Descent (PGD)** PGD [12] is almost the same as BIM, the only difference being that PGD initialize  $x'_0$  as a random point in the  $\varepsilon$ -neighbourhood of  $x$ .

**Momentum Iterative Method (MIM)** MIM is an extension of BIM. It updates the gradient  $g_i$  with the momentum  $\mu$  as follows [31]:

$$x'_i = \text{clip}_{x, \varepsilon} \left( x'_{i-1} + \frac{\varepsilon}{r} \cdot \text{sign}(g_i) \right) \quad (4)$$

where  $g_i = \mu g_{i-1} + \frac{\nabla_x \ell(x'_{i-1}, y)}{\|\nabla_x \ell(x'_{i-1}, y)\|_1}$ , and  $\|\cdot\|_1$  denotes the  $L_1$  norm.

## 2.4 On techniques to generate soft labels

Label smoothing is perhaps the most popularly used technique to generate soft labels [32,4,33,34]. Although it is simple, it has been demonstrated as an effective approach to improve the accuracy of deep learning predictions. For example, Szegedy et al. propose generating soft labels by averaging the one-hot vector and a uniform distribution over labels [4]. Fu et al. study the effect of label smoothing on adversarial training and find that adversarial training with the aid of label smoothing can enhance model robustness against gradient-based attacks [35]. Wang et al. propose an adaptive label smoothing approach capable of adaptively estimating a target label distribution [36]. Guo et al. propose a label confusion model (LCM) to improve text classification performance [26], which we adapt here for CLDL and generating soft labels for adversarial ensemble prediction.

## 3 CLDL Assisted Ensemble Training

Here we describe our CLDL based ensemble training approach in detail. We present a pseudo-code implementation of our approach in Algorithm 1 and a conceptual illustration in Fig.2. For ease of presentation, we will use an example of an ensemble consisting of  $N = 2$  member models.

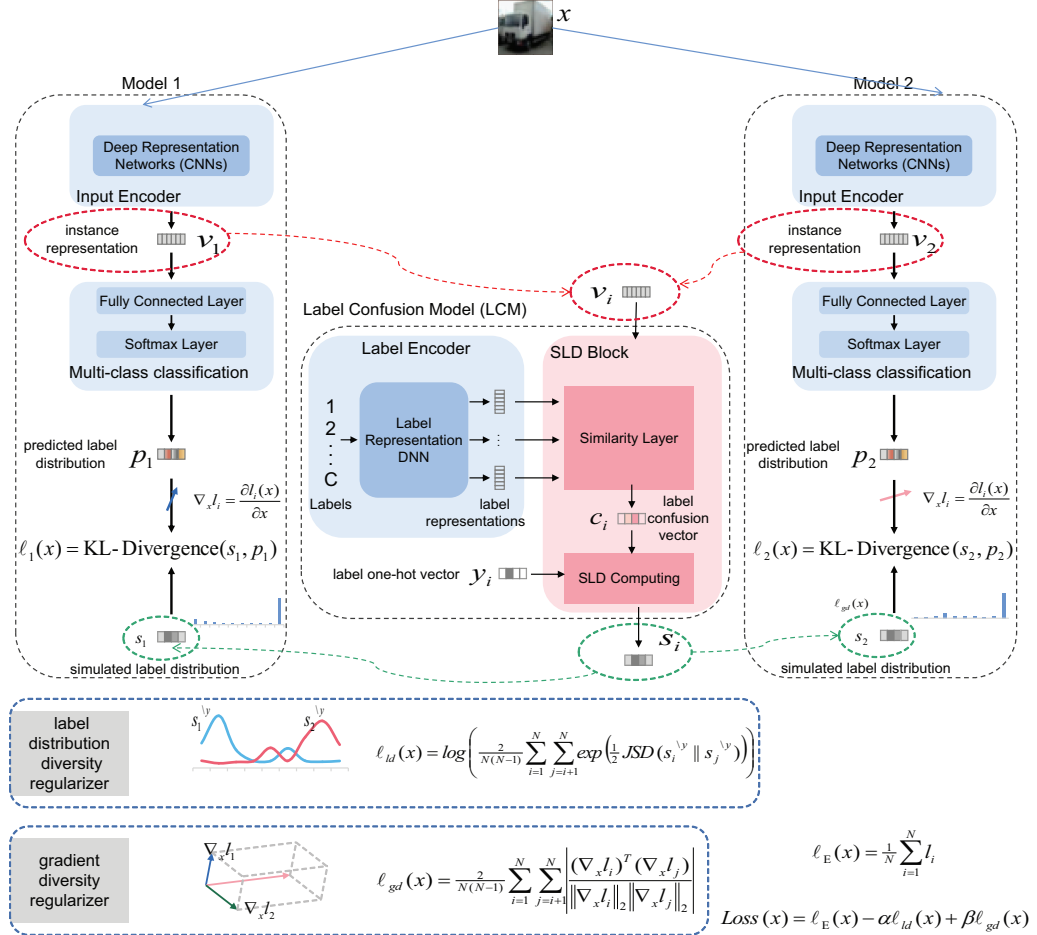
**Algorithm 1** CLDL assisted ensemble training for an ensemble of  $N$  sub-models

- 
- 1: Initialization: Initialize  $N$  individual models  $\{\mathcal{F}_i(x, \theta_i)\}_{i \in [N]}$ , where  $[N] = \{1, 2, \dots, N\}$ , and the label confusion model  $\text{LCM}(v, y, \theta)$ , where  $\theta$  denotes the model parameter. Input the training dataset  $\mathcal{D}_{train} = \{(x_j, y_j)\}_{j \in [M]}$  to the algorithm. Set the number of training epochs  $\mathcal{T}$ , the learning rates  $\epsilon_i$  and  $\epsilon$ ,  $\forall i \in [N]$ , the iteration number  $\mathcal{IN}$ , and the model indicator set  $\mathcal{I} = [N]$ .
  - 2: **for** current epoch  $t = 1$  to  $\mathcal{T}$  **do**
  - 3:   **for**  $iter = 1$  to  $\mathcal{IN}$  **do**
  - 4:     Sample a mini-batch  $\mathcal{D}_{iter}$  from  $\mathcal{D}_{train}$
  - 5:     **for**  $i$  in  $\mathcal{I}$  **do**
  - 6:       Obtain the instance representation  $\{v_j(x_j, \theta_i)\}_{x_j \in \mathcal{D}_{iter}}$  from the outputs of the last Linear layer of  $\mathcal{F}_i(x_j, \theta_i)$ .
  - 7:       Obtain the predicted label distribution  $\{p_j(x_j, \theta_i)\}_{x_j \in \mathcal{D}_{iter}}$  from the outputs of soft-max layer of  $\mathcal{F}_i(x_j, \theta_i)$ .
  - 8:       Obtain the simulated label distribution  $\{s_j(x_j, \theta_i)\}_{x_j \in \mathcal{D}_{iter}}$  from  $\text{LCM}(v_j, y_j, \theta)$  by Eqn. (6).
  - 9:       Calculate loss  $\ell_i(x_j, \theta_i)_{x_j \in \mathcal{D}_{iter}}$  by Eqn. (7).
  - 10:       Calculate the gradients of the loss  $(\nabla_{x_j} \ell_i)_{x_j \in \mathcal{D}_{iter}}$ .
  - 11:     **end for**
  - 12:     Calculate the label distribution similarity loss  $\ell_{ld}(x_j)_{x_j \in \mathcal{D}_{iter}}$  by Eqn. (9)
  - 13:     Calculate the model loss gradient consistency loss  $\ell_{gd}(x_j)_{x_j \in \mathcal{D}_{iter}}$  by Eqn. (10)
  - 14:     Calculate the combined diversity promoting loss  $\ell_{\mathcal{F}, \mathcal{G}}(x_j)_{x_j \in \mathcal{D}_{iter}}$  by Eqn. (11)
  - 15:     Obtain the final loss on  $\mathcal{D}_{iter}$ , denoted by  $\mathcal{L}_{CLDL}^{iter}$ , using Eqn.(12).
  - 16:     **for**  $i$  in  $\mathcal{I}$  **do**
  - 17:       Update  $\theta^i \leftarrow \theta^i - \epsilon_i \nabla_{\theta^i} \mathcal{L}_{CLDL}^{iter}|_{\{\theta_i\}_{i \in [N]}}$
  - 18:     **end for**
  - 19:     Update  $\theta \leftarrow \theta - \epsilon \nabla_{\theta} \mathcal{L}_{CLDL}^{iter}|_{\{\theta\}}$  for  $\text{LCM}(v, y, \theta)$ .
  - 20:   **end for**
  - 21: **end for**
  - 22: **return** The parameters  $\theta^i$  and  $\theta$ , where  $i \in [N]$ .
- 

Our model is mainly composed of two parts: an ensemble of  $N$  sub-models ( $\{\mathcal{F}_i(x, \theta_i)\}_{i \in [N]}$ , where  $[N] = \{1, 2, \dots, N\}$ ) and a label confusion model (LCM) adapted from [26]. Each sub-model in the ensemble consists of an input convolutional neural network (CNN) encoder followed by a fully connected classifier, which can be any main stream DNN based image classifier. As shown in Fig.2, an image instance ( $x$ ) is fed into the input-encoder, which generates an image representation  $v_i$ , where  $i$  is the sub-model index. Then  $v_i$  is fed into the fully connected classifier to predict the label distribution of this image. The above operations can be formulated as follows:

$$\begin{aligned}
 v_i &= \mathcal{F}_i^{encoder}(x) \\
 p_i &= \text{softmax}(Wv_i + b)
 \end{aligned}
 \tag{5}$$

where  $\mathcal{F}_i^{encoder}(\cdot)$  is the output of input-encoder of  $\mathcal{F}_i$  which transforms  $x$  to  $v_i$ ,  $W$  and  $b$  are weights and the bias of the fully connect layer that transforms  $v_i$  to the predicted label distribution (PLD)  $p_i$ .



Ensemble Diversity Training

**Figure 2.** The proposed CLDL assisted ensemble training method. Here we take an ensemble model that consists of two member models as an example for ease of illustration. Given an image instance  $x$ , the label confusion model (LCM) in the middle, which is adapted from [26], is used to generate a soft label  $s_i$  for the  $i$ th sub-model. Two types of diversity regularizers that are based on the label distribution given the soft labels and the gradient are combined to generate the finally used ensemble diversity regularizer. See the text in Section 3 for more details. The LCM module is drawn referring to Fig.1 of [26]. Note that the model of [26] is used for text classification, while here it is adapted to an ensemble model for image classification under adversarial attacks.

The LCM consists of two parts: a label encoder and a simulated label distribution (SLD) computation block. The label encoder is a deep neural network used to generate the label representation matrix [26]. The SLD computation block comprises a similarity layer and an SLD computation layer. The similarity layer takes the label representation matrix and the current instance’s representation as inputs, computes the dot product similarities between the image instance and each image class label, then feeds the similarity values into a soft-max activation layer that outputs the label confusion vector (LCV). The LCV captures the conditional dependencies among the image classes through the computed similarities between the instance representation and the label representations. The LCV is instance-dependent, meaning it considers the dependency relationships among all image class labels conditional on a specific image instance. In the following SLD computation layer, the one-hot vector formed hard label  $y_i$  is added to the LCV with a controlling parameter  $\gamma$ , which is then normalized by a soft-max function that generates the SLD. The controlling parameter  $\gamma$  decides how much of the one-hot vector will be changed by the LCV. The above operations can be formulated as follows:

$$\begin{aligned} Vec^{(l)} &= f^L(l) = f^L([l_1, l_2, \dots, l_C]) = [Vec_{c_1}^{(l)}, Vec_{c_2}^{(l)}, \dots, Vec_C^{(l)}] \\ c_i &= \text{softmax}(v_i^\top Vec^{(l)}W + b) \\ s_i &= \text{softmax}(\gamma y_i + c_i) \end{aligned} \quad (6)$$

where  $f^L$  is the label encoder function to transfer labels  $l = [l_1, l_2, \dots, l_C]$  to the label representation matrix  $Vec^{(l)}$ ,  $C$  the number of image classes,  $f^L$  is implemented by an embedding lookup layer followed by a DNN,  $c_i$  the LCV and  $s_i$  the SLD. The SLD is then viewed as a soft label that replaces the original hard label for model training.

Note that the SLD  $s_i$  and the predicted label vector  $p_i$  are both probability measures. We use the Kullback-Leibler (KL) divergence [37] to measure their difference:

$$\ell_i(x) = KL(s_i, p_i) = \sum_{c=1}^C s_i^c \log\left(\frac{s_i^c}{p_i^c}\right) \quad (7)$$

The LCM is trained by minimizing the above KL divergence, whose value depends on the semantic representation of the image instance  $v_i$  and the soft label  $s_i$  given by the LCM.

### 3.1 Diversity Promoting Loss Design

Here we present our design of the diversity promoting loss used in our approach.

**Soft label diversity** For an input  $(x, y)$  in the training dataset, we define the soft label diversity based on the non-maximal value of the SLD of each sub-model. Specifically, let  $s_i^{\setminus y}$  be a  $(C - 1) \times 1$  vector constructed by excluding the maximal value from the SLD corresponding to model  $\mathcal{F}_i(x, \theta)$ . Then we use

the Jensen-Shannon divergence (JSD) [38] to measure the difference between a pair of, say the  $i$ th and the  $j$ th member models, in terms of their predicted soft labels, as follows

$$\text{JSD}(s_i^y \| s_j^y) = \frac{1}{2} \left( KL \left( s_i^y, \frac{s_i^y + s_j^y}{2} \right) + KL \left( s_j^y, \frac{s_i^y + s_j^y}{2} \right) \right) \quad (8)$$

From Eqns. (6) and (8), we see that  $\text{JSD}(s_i^y \| s_j^y)$  monotonically increases with  $\text{JSD}(c_i^y \| c_j^y)$ . A large JSD indicates a misalignment between the SLDs of the two involved sub-models given the image instance  $x$ . Given  $x$  and an ensemble of  $N$  models, we define a loss item as follows

$$\ell_{ld}(x) = \log \left( \frac{2}{N(N-1)} \sum_{i=1}^N \sum_{j=i+1}^N \exp \left( \text{JSD}(s_i^y \| s_j^y) \right) \right) \quad (9)$$

which will be included in the final loss function Eqn.(12) used for training the model ensemble. It plays a vital role in promoting the member models' diversity concerning their pre-dicted soft labels given any input instance.

It is worth noting that we only consider the non-maximal values of the SLDs in Eqn.(8) following [22]. By doing so, promoting the diversity among the sub-models does not affect the ensemble's prediction accuracy for benign inputs. However, it can lower the transferability of attacks among the sub-models.

**Gradient diversity** Following [25,21], we consider the sub-models' diversity in terms of gradients associated with them. Given an image instance  $x$  and an ensemble of  $N$  models, we define the gradient diversity loss item as follows

$$\ell_{gd}(x) = \frac{2}{N(N-1)} \sum_{i=1}^N \sum_{j=i+1}^N CS(\nabla_x l_i, \nabla_x l_j) = \frac{2}{N(N-1)} \sum_{i=1}^N \sum_{j=i+1}^N \left| \frac{(\nabla_x l_i)^T (\nabla_x l_j)}{\|\nabla_x l_i\|_2 \|\nabla_x l_j\|_2} \right| \quad (10)$$

which will also be included in the final loss function Eqn.(12).

**The Combined Diversity Promoting Loss** Combining the above soft label and gradient diversity loss items, we propose our CLDL based ensemble diversity loss function. For a pair of member models ( $\mathcal{F}$  and  $\mathcal{G}$ ), given an input instance  $x$ , this diversity promoting loss function is

$$\ell_{\mathcal{F}, \mathcal{G}, x} = -\alpha \ell_{ld}(x) + \beta \ell_{gd}(x), \quad (11)$$

where  $\alpha, \beta \geq 0$  are hyper-parameters that balance the effects of the soft label based and the gradient based diversity loss items.

### 3.2 CLDL based Ensemble Model Training

We train our ensemble model by minimizing the training loss function defined as follows

$$\text{Loss}(x) = \ell_{\text{E}}(x) + \ell_{\mathcal{F},\mathcal{G},x} = \left(\frac{1}{N} \sum_{i=1}^N \ell_i\right) - \alpha \ell_{id}(x) + \beta \ell_{gd}(x) \quad (12)$$

where  $\ell_{\text{E}}(x) = \frac{1}{N} \sum_{i=1}^N \ell_i$  refers to the average of the KL-divergence losses of the member models. See Fig.2 for the definition of the KL loss of the member models. By minimizing the above loss function, we simultaneously learn the soft labels given by each sub-model, promote the diversity among the sub-models in terms their predicted soft labels and their gradients, and minimize the KL-divergence loss of each sub-model.

## 4 Experiments

### 4.1 Datasets and Competitor Methods

We conducted our experiments on the widely-used image datasets MNIST [39], Fasion-MNIST (F-MNIST) [40], and CIFAR-10 [41]. For each dataset, we used its training set for ensemble training. We set the hyper-parameters of our algorithm based on 1,000 test images randomly sampled from the testing set and used the remaining data in the testing set for performance evaluation.

We compared the performance of our algorithm with competitor methods, including a baseline method that trains the model ensemble without the use of any defense mechanism and four popularly used ensemble training methods: the adaptive diversity promoting (ADP) algorithm, the gradient alignment loss (GAL) method, the diversi-fying vulnerabilities for enhanced robust generation of ensembles (DVERGE) meth-od, and the transferability reduced smooth (TRS) method. We used ResNet-20 as the basic model structure of the sub-models and averaged the output probabilities given by the softmax layer of the member models to yield the final prediction.

### 4.2 Optimizer for Training

We use Adam [42] as the optimizer for ensemble training with an initial learning rate of  $10^{-3}$ , and a weight decaying parameter of  $10^{-4}$ . For our CLDL-based approach, we trained the ensemble for 200 epochs, multiplied the learning rate by 0.1 twice at the 100th and 150th epochs, respectively. We set the batch size to 128 and used normalization, random cropping, and flipping-based data augmentations for dataset CIFAR-10. We considered two ensemble sizes, 3 and 5, in our experiments. To make a fair comparison, we trained ADP, GAL, DVERGE, and TRS under a similar training setup described above. We used the AdverTorch [43] library for simulating adversarial attacks.

### 4.3 White-box Attacks

We considered four basic white-box adversarial attacks, namely FGSM, BIM, MIM, and PGD for simulating black-box attacks used in our experiments. For each attack type, we considered four different perturbation scales ( $\epsilon$ ) ranging from 0.01 to 0.04. We set the number of attack iterations at 10 and set the step size to be  $\epsilon/5$  for BIM, MIM and PGD. Each experiment was run five times independently, and the results were averaged for performance comparison. We simulated the white-box attacks by treating the whole ensemble, other than one of the individual sub-models, as the target model to be attacked.

### 4.4 Black-box Attacks

We considered black-box attacks, in which the attacker has no knowledge about the target model, including its architecture and parameters. The attacker designs adversarial examples based on several surrogate models. We simulated black-box attacks with our ensemble model as the target by creating white-box adversarial attacks based on a surrogate ensemble model that has the same architecture as the true target ensemble and is trained on the same dataset using the same training routine.

We trained the surrogate ensemble model consisting of 3- or 5-member sub-models by minimizing a standard ensemble cross-entropy loss function. For each type of attack mentioned above, we evaluated the robustness of the involved training methods under black-box attacks with four different perturbation scales ( $\epsilon$ ) 0.01, 0.02, 0.03 and 0.04. We set the number of attack iterations at 10, and the step size at  $\epsilon/5$  for BIM, MIM and PGD based attacks. Following [44], we generate adversarial examples using the cross-entropy loss and the CW loss [11].

### 4.5 Experimental Results for Black-box Adversarial Attacks

In our experiments, we used classification accuracy as the performance metric, which is the ratio of the number of correctly predicted adversarial instances to the total number of adversarial instances. We conducted random re-trainings of the model in our experiments, and the reported values are averages of multiple ( $> 3$ ) independent tests. Our code is open-sourced to support reproducibility of these results.

**CIFAR-10** Here we present our experimental results on CIFAR-10 in Tables 1 and 2. Note that, in all tables shown below,  $CLDL_{a,b,c}$  denotes our CLDL based algorithm with hyper-parameters, namely  $\gamma$  in Eqn.(6),  $\alpha$  and  $\beta$  in Eqn.(12), set to be  $a$ ,  $b$ , and  $c$ , respectively.  $\epsilon$  refers to the perturbation scale of the attack. As is shown, our CLDL based algorithm performs best for almost all attacks considered, compared to the other methods, especially when the perturbation scale is large.

We also investigate the effects of the soft label diversity based loss and the gradient diversity based one on the performance of our algorithm. See the result

**Table 1.** Classification accuracy (%) on the CIFAR-10 dataset for four types of black-box attacks. The ensemble consists of 3 ReNets-20 member models.  $\epsilon$  refers to the perturbation scale for the attack.

| CIFAR-10 | $\epsilon$ | ADP   | GAL          | DVERGE | TRS   | $CLDL_{4,2,4}$ | $CLDL_{4,0.5,4}$ |
|----------|------------|-------|--------------|--------|-------|----------------|------------------|
| BIM      | 0.01       | 45.43 | 92.61        | 89.66  | 87.86 | <b>92.77</b>   | <b>92.77</b>     |
|          | 0.02       | 9.74  | 83.59        | 75.41  | 71.17 | <b>85.21</b>   | 83.66            |
|          | 0.03       | 2.01  | 73.02        | 59.24  | 53.74 | <b>75.76</b>   | 72.97            |
|          | 0.04       | 0.47  | 62.32        | 42.27  | 37.87 | <b>66.47</b>   | 62.38            |
| FGSM     | 0.01       | 67.03 | 93.47        | 91.20  | 90.37 | <b>93.49</b>   | 93.47            |
|          | 0.02       | 40.58 | 84.62        | 78.68  | 77.59 | <b>86.21</b>   | 85.48            |
|          | 0.03       | 26.41 | 75.93        | 65.37  | 64.12 | <b>77.94</b>   | 76.04            |
|          | 0.04       | 18.25 | 66.15        | 51.40  | 51.04 | <b>69.93</b>   | 66.95            |
| MIM      | 0.01       | 41.65 | 91.11        | 87.52  | 85.39 | <b>91.29</b>   | 91.08            |
|          | 0.02       | 7.37  | 76.92        | 65.85  | 61.80 | <b>78.98</b>   | 77.01            |
|          | 0.03       | 1.13  | 59.75        | 40.35  | 38.01 | <b>63.84</b>   | 59.89            |
|          | 0.04       | 0.30  | 43.48        | 19.77  | 20.24 | <b>48.27</b>   | 43.06            |
| PGD      | 0.01       | 46.20 | <b>92.41</b> | 89.36  | 88.06 | 92.18          | 92.25            |
|          | 0.02       | 9.23  | 83.46        | 76.08  | 72.07 | <b>84.81</b>   | 83.68            |
|          | 0.03       | 1.55  | 74.67        | 61.28  | 55.12 | <b>77.34</b>   | 75.04            |
|          | 0.04       | 0.35  | 65.46        | 44.72  | 39.23 | <b>70.64</b>   | 67.09            |

**Table 2.** Classification accuracy (%) on the CIFAR-10 dataset for four types of black-box attacks. The ensemble consists of 5 ReNets-20 member models.

| CIFAR-10 | $\epsilon$ | ADP   | GAL   | DVERGE       | TRS   | $CLDL_{4,2,4}$ | $CLDL_{4,0.5,4}$ |
|----------|------------|-------|-------|--------------|-------|----------------|------------------|
| BIM      | 0.01       | 45.28 | 92.22 | 93.32        | 91.17 | <b>93.73</b>   | 92.89            |
|          | 0.02       | 9.50  | 81.69 | 85.27        | 80.15 | <b>85.71</b>   | 84.58            |
|          | 0.03       | 1.79  | 69.68 | 75.72        | 67.93 | <b>75.93</b>   | 75.56            |
|          | 0.04       | 0.44  | 57.21 | 64.59        | 55.95 | 65.39          | <b>65.8</b>      |
| FGSM     | 0.01       | 68.49 | 93.33 | 94.22        | 92.65 | <b>94.47</b>   | 93.54            |
|          | 0.02       | 43.02 | 84.13 | 86.79        | 83.30 | <b>87.06</b>   | 85.92            |
|          | 0.03       | 27.76 | 74.15 | 77.56        | 72.24 | <b>78.79</b>   | 78.3             |
|          | 0.04       | 19.36 | 64.32 | 67.10        | 61.08 | <b>69.93</b>   | 69.68            |
| MIM      | 0.01       | 41.77 | 90.50 | 91.92        | 89.53 | <b>92.17</b>   | 91.4             |
|          | 0.02       | 7.42  | 73.95 | <b>79.69</b> | 73.33 | 79.33          | 78.67            |
|          | 0.03       | 1.16  | 55.09 | 62.87        | 54.63 | <b>63.24</b>   | 62.93            |
|          | 0.04       | 0.25  | 37.87 | 44.19        | 38.76 | <b>47.16</b>   | 46.62            |
| PGD      | 0.01       | 46.50 | 92.22 | <b>93.34</b> | 91.29 | 92.92          | 92.02            |
|          | 0.02       | 9.43  | 81.85 | 85.60        | 80.24 | <b>85.92</b>   | 84.45            |
|          | 0.03       | 1.54  | 71.89 | 77.59        | 68.25 | <b>78.07</b>   | 76.87            |
|          | 0.04       | 0.29  | 61.60 | 68.53        | 55.45 | <b>70.05</b>   | 69.78            |

in Table 3. As is shown,  $CLDL_{4,2,4}$  gives the best results. By comparing the result of  $CLDL_{4,2,4}$  to that of  $CLDL_{4,0.5,4}$ , we find a performance gain given by the soft label diversity based loss. By comparing the result of  $CLDL_{4,2,4}$  to that of  $CLDL_{4,2,0}$ , we verify the contribution of the gradient diversity based loss.

**Table 3.** Classification accuracy (%) given by an ensemble model consisting of 3 ReNets-20 member models trained with our CLDL based algorithm with different hyper-parameter settings against black-box attacks on the CIFAR-10 dataset.

| CIFAR-10 | $\epsilon$ | CLDL <sub>4,0,0</sub> | CLDL <sub>4,1,0</sub> | CLDL <sub>4,2,0</sub> | CLDL <sub>4,4,0</sub> | CLDL <sub>4,1,2</sub> | CLDL <sub>4,2,2</sub> | CLDL <sub>4,0.5,4</sub> | CLDL <sub>4,2,4</sub> |
|----------|------------|-----------------------|-----------------------|-----------------------|-----------------------|-----------------------|-----------------------|-------------------------|-----------------------|
| BIM      | 0.01       | 89.97                 | 89.66                 | 89.82                 | 89.78                 | 92.76                 | 92.62                 | <b>92.77</b>            | <b>92.77</b>          |
|          | 0.02       | 74.01                 | 74.18                 | 74.2                  | 74.42                 | 83.43                 | 82.97                 | 83.66                   | <b>85.21</b>          |
|          | 0.03       | 57.1                  | 56.62                 | 56.78                 | 56.92                 | 73.02                 | 72.64                 | 72.97                   | <b>75.76</b>          |
|          | 0.04       | 40.11                 | 39.63                 | 40.63                 | 40.53                 | 61.8                  | 61.69                 | 62.38                   | <b>66.47</b>          |
| FGSM     | 0.01       | 91.53                 | 91.07                 | 91.01                 | 91.12                 | <b>93.5</b>           | 93.2                  | 93.47                   | 93.49                 |
|          | 0.02       | 78.64                 | 78.63                 | 78.78                 | 78.51                 | 84.79                 | 84.62                 | 85.48                   | <b>86.21</b>          |
|          | 0.03       | 64.83                 | 64.37                 | 65.22                 | 64.37                 | 76.05                 | 76.24                 | 76.04                   | <b>77.94</b>          |
|          | 0.04       | 52.36                 | 51.87                 | 53.11                 | 52.16                 | 66.55                 | 67.42                 | 66.95                   | <b>69.93</b>          |
| MIM      | 0.01       | 87.64                 | 87.18                 | 87.39                 | 87.26                 | 91.22                 | 90.73                 | 91.08                   | <b>91.29</b>          |
|          | 0.02       | 63.63                 | 63.24                 | 63.79                 | 63.86                 | 76.16                 | 76.3                  | 77.01                   | <b>78.98</b>          |
|          | 0.03       | 39.03                 | 38.62                 | 39.29                 | 38.82                 | 58.9                  | 59.25                 | 59.89                   | <b>63.84</b>          |
|          | 0.04       | 20.84                 | 20.29                 | 21.5                  | 21.42                 | 41.79                 | 43.07                 | 43.06                   | <b>48.27</b>          |
| PGD      | 0.01       | 90.24                 | 89.74                 | 89.76                 | 89.75                 | <b>92.26</b>          | 92.09                 | 92.25                   | 92.18                 |
|          | 0.02       | 75.54                 | 75.66                 | 75.48                 | 75.69                 | 83.25                 | 82.81                 | 83.68                   | <b>84.81</b>          |
|          | 0.03       | 60.63                 | 60.03                 | 60.55                 | 60.13                 | 74.53                 | 74.45                 | 75.04                   | <b>77.34</b>          |
|          | 0.04       | 46.97                 | 46.2                  | 46.68                 | 46.41                 | 66.03                 | 65.95                 | 67.09                   | <b>70.64</b>          |

**Table 4.** Classification accuracy (%) given by an ensemble model consisting of 3 LeNet-5 member models trained with our CLDL based algorithm against black-box attacks on the MNIST dataset.

| MNIST | $\epsilon$ | ADP   | GAL   | DVERGE | TRS   | CLDL <sub>3,4,4</sub> | CLDL <sub>3,2,1</sub> |
|-------|------------|-------|-------|--------|-------|-----------------------|-----------------------|
| BIM   | 0.1        | 90.18 | 87.34 | 90.24  | 92.5  | <b>94.48</b>          | 94.22                 |
|       | 0.15       | 60.38 | 55.61 | 61.21  | 76.63 | <b>85.64</b>          | 81.42                 |
|       | 0.2        | 23.23 | 28.5  | 21.17  | 46.16 | <b>65.11</b>          | 51.59                 |
|       | 0.25       | 5.32  | 11.06 | 2.53   | 17.42 | <b>32.81</b>          | 22.95                 |
| FGSM  | 0.1        | 93.29 | 90.77 | 93.51  | 94.55 | 95.43                 | <b>95.5</b>           |
|       | 0.15       | 79.58 | 69.94 | 80.75  | 86.21 | <b>89.82</b>          | 88.56                 |
|       | 0.2        | 52.99 | 47.35 | 55.98  | 70.64 | <b>78.39</b>          | 72.73                 |
|       | 0.25       | 27.38 | 30.13 | 27.78  | 48.1  | <b>57.51</b>          | 46.77                 |
| MIM   | 0.1        | 90.21 | 85.82 | 90.52  | 92.31 | <b>94.25</b>          | 94.07                 |
|       | 0.15       | 63.05 | 53.72 | 63.67  | 76.81 | <b>85.31</b>          | 81.56                 |
|       | 0.2        | 24.69 | 27.49 | 23.88  | 46.83 | <b>65.1</b>           | 51.33                 |
|       | 0.25       | 5.58  | 10.64 | 3.16   | 16.58 | <b>30.44</b>          | 21.34                 |
| PGD   | 0.1        | 89.66 | 84.87 | 89.82  | 91.91 | 93.75                 | <b>93.84</b>          |
|       | 0.15       | 56.83 | 47.69 | 57.86  | 73.01 | <b>83.5</b>           | 78.92                 |
|       | 0.2        | 19.42 | 21.69 | 17.32  | 39.19 | <b>58.94</b>          | 46.91                 |
|       | 0.25       | 3.06  | 6.44  | 1.05   | 11.71 | <b>24.81</b>          | 16.65                 |

**Table 5.** Robust accuracy (%) of an ensemble of 5 LeNet-5 models against black-box attacks on the MNIST dataset

| MNIST | $\epsilon$ | ADP   | GAL   | DVERGE | TRS   | CLDL <sub>3,4,4</sub> | CLDL <sub>3,2,1</sub> |
|-------|------------|-------|-------|--------|-------|-----------------------|-----------------------|
| BIM   | 0.1        | 88.43 | 90.26 | 89.49  | 94.01 | <b>95.01</b>          | 93.98                 |
|       | 0.15       | 53.68 | 66.19 | 60.83  | 82.77 | <b>87.18</b>          | 78.76                 |
|       | 0.2        | 18.98 | 34.1  | 23.04  | 55.12 | <b>68.76</b>          | 51.46                 |
|       | 0.25       | 2.21  | 12.02 | 4.01   | 22.2  | <b>40.58</b>          | 25.3                  |
| FGSM  | 0.1        | 92.23 | 93.03 | 92.88  | 95.41 | 95.9                  | 95.62                 |
|       | 0.15       | 75.07 | 79.74 | 80.23  | 88.85 | <b>89.86</b>          | 88.43                 |
|       | 0.2        | 46.26 | 58.21 | 54.71  | 76.11 | <b>76.95</b>          | 71.07                 |
|       | 0.25       | 22.41 | 35.67 | 29.5   | 54.6  | 52.6                  | 44.93                 |
| MIM   | 0.1        | 89.06 | 89.62 | 89.84  | 93.96 | <b>94.68</b>          | 93.96                 |
|       | 0.15       | 56.8  | 66.79 | 63.58  | 82.61 | <b>85.96</b>          | 78.68                 |
|       | 0.2        | 21.1  | 35.18 | 26.19  | 56.63 | <b>65.32</b>          | 50.11                 |
|       | 0.25       | 3.02  | 12.37 | 5.33   | 22.55 | <b>34.31</b>          | 22.36                 |
| PGD   | 0.1        | 87.83 | 88.69 | 89.11  | 93.53 | <b>94.4</b>           | 93.49                 |
|       | 0.15       | 50.51 | 60.26 | 57.6   | 81.19 | <b>85.08</b>          | 74.77                 |
|       | 0.2        | 15.33 | 27.47 | 19.45  | 50.15 | <b>63.35</b>          | 45.58                 |
|       | 0.25       | 0.97  | 6.64  | 2.19   | 17.06 | <b>31.88</b>          | 18.38                 |

**MNIST** In Tables 4 and 5, we show the classification accuracy (%) results for an ensemble of 3 and 5 LeNet-5 member models [45] on the MNIST dataset. We find that again our algorithm outperforms its competitors significantly.

**Table 6.** Classification accuracy (%) of an ensemble of 3 LeNet-5 models against black-box attacks on the F-MNIST dataset.

| <b>F-MNIST</b> | $\epsilon$ | ADP   | GAL          | DVERGE | TRS          | <i>CLDL</i> <sub>3,2,4</sub> |
|----------------|------------|-------|--------------|--------|--------------|------------------------------|
| BIM            | 0.08       | 38.38 | 54.43        | 39.42  | <b>54.71</b> | 54.19                        |
|                | 0.1        | 28.39 | 44.37        | 28.16  | 44.61        | <b>44.99</b>                 |
|                | 0.15       | 10.55 | 22.63        | 10.58  | 25.06        | <b>27.84</b>                 |
|                | 0.2        | 1.78  | 7.10         | 2.69   | 10.95        | <b>13.98</b>                 |
| FGSM           | 0.08       | 48.25 | 62.77        | 52.39  | <b>62.83</b> | 61.99                        |
|                | 0.1        | 40.09 | <b>54.22</b> | 42.80  | 53.64        | 53.87                        |
|                | 0.15       | 23.24 | 36.09        | 25.41  | 37.63        | <b>38.49</b>                 |
|                | 0.2        | 9.82  | 15.85        | 13.33  | 23.45        | <b>25.67</b>                 |
| MIM            | 0.08       | 38.24 | 52.83        | 39.58  | <b>53.46</b> | 52.88                        |
|                | 0.1        | 28.41 | 42.44        | 28.19  | 43.10        | <b>43.41</b>                 |
|                | 0.15       | 9.17  | 19.61        | 9.98   | 23.01        | <b>25.20</b>                 |
|                | 0.2        | 1.01  | 3.44         | 2.33   | 7.84         | <b>9.75</b>                  |
| PGD            | 0.08       | 37.74 | 52.34        | 39.17  | <b>52.86</b> | 51.65                        |
|                | 0.1        | 27.75 | 41.71        | 28.15  | <b>42.38</b> | 42.23                        |
|                | 0.15       | 8.69  | 18.78        | 9.67   | 22.44        | <b>24.75</b>                 |
|                | 0.2        | 1.08  | 3.52         | 2.24   | 8.25         | <b>10.91</b>                 |

**Table 7.** Classification accuracy (%) of an ensemble of 5 LeNet-5 models on the F-MNIST dataset

| <b>F-MNIST</b> | $\epsilon$ | ADP   | GAL   | DVERGE | TRS          | <i>CLDL</i> <sub>3,2,4</sub> |
|----------------|------------|-------|-------|--------|--------------|------------------------------|
| BIM            | 0.08       | 38.01 | 52.62 | 41.36  | 60.30        | <b>61.37</b>                 |
|                | 0.1        | 28.57 | 42.47 | 29.67  | 51.10        | <b>51.72</b>                 |
|                | 0.15       | 10.83 | 23.04 | 11.15  | 33.67        | <b>35.46</b>                 |
|                | 0.2        | 2.01  | 8.86  | 2.63   | 20.48        | <b>24.58</b>                 |
| FGSM           | 0.08       | 48.36 | 62.53 | 54.13  | 65.65        | <b>67.90</b>                 |
|                | 0.1        | 39.94 | 54.14 | 44.80  | 58.09        | <b>59.78</b>                 |
|                | 0.15       | 23.00 | 36.65 | 27.28  | 43.66        | <b>45.69</b>                 |
|                | 0.2        | 9.98  | 19.49 | 14.44  | 31.91        | <b>32.71</b>                 |
| MIM            | 0.08       | 38.22 | 52.16 | 41.69  | 58.93        | <b>59.18</b>                 |
|                | 0.1        | 28.65 | 42.23 | 30.20  | 49.41        | <b>49.48</b>                 |
|                | 0.15       | 9.75  | 20.97 | 11.27  | 31.79        | <b>33.15</b>                 |
|                | 0.2        | 1.26  | 4.94  | 2.12   | 17.11        | <b>18.71</b>                 |
| PGD            | 0.08       | 37.76 | 51.56 | 41.11  | <b>59.06</b> | 58.28                        |
|                | 0.1        | 27.86 | 41.03 | 29.50  | <b>49.18</b> | 47.99                        |
|                | 0.15       | 9.39  | 20.45 | 10.14  | 31.27        | <b>32.97</b>                 |
|                | 0.2        | 1.39  | 5.99  | 1.97   | 18.00        | <b>20.38</b>                 |

**F-MNIST** In Tables 6 and 7, we present results associated with the F-MNIST dataset. As is shown, among all methods involved, our CLDL algorithm ranks number 1 for 10 times. TRS and GAL have 5 times and one time to rank number 1, respectively.

## 5 Conclusion

In this paper, we proposed a novel adversarial ensemble training approach that leverages conditional label dependency learning. In contrast to existing methods that encode image classes with one-hot vectors, our algorithm can learn and exploit the conditional relationships between labels during member model training. Experimental results demonstrate that our approach is more robust against black-box adversarial attacks than state-of-the-art methods.

## Acknowledgment

This work was supported by Research Initiation Project (No.2021KB0PI01) and Exploratory Research Project (No.2022RC0AN02) of Zhejiang Lab.

## References

1. K. He, X. Zhang, S. Ren, and J. Sun, “Deep residual learning for image recognition,” in *Proc. of the IEEE Conf. on Computer Vision and Pattern Recognition*, 2016, pp. 770–778.
2. A. Krizhevsky, I. Sutskever, and G. E. Hinton, “Imagenet classification with deep convolutional neural networks,” *Advances in neural information processing systems*, vol. 25, 2012.
3. O. Russakovsky, J. Deng, H. Su, J. Krause, S. Satheesh, S. Ma, Z. Huang, A. Karpathy, A. Khosla, and M. Bernstein, “Imagenet large scale visual recognition challenge,” *International Journal of Computer Vision*, vol. 115, no. 3, pp. 211–252, 2015.
4. C. Szegedy, V. Vanhoucke, S. Ioffe, J. Shlens, and Z. Wojna, “Rethinking the inception architecture for computer vision,” in *Proc. of the IEEE Conf. on Computer Vision and Pattern Recognition*, 2016, pp. 2818–2826.
5. A. Graves and N. Jaitly, “Towards end-to-end speech recognition with recurrent neural networks,” in *International conference on machine learning*. PMLR, 2014, pp. 1764–1772.
6. A. Hannun, C. Case, J. Casper, B. Catanzaro, G. Diamos, E. Elsen, R. Prenger, S. Satheesh, S. Sengupta, A. Coates *et al.*, “Deep speech: Scaling up end-to-end speech recognition,” *arXiv preprint arXiv:1412.5567*, 2014.
7. I. Sutskever, O. Vinyals, and Q. V. Le, “Sequence to sequence learning with neural networks,” *Advances in neural information processing systems*, vol. 27, 2014.
8. T. Young, D. Hazarika, S. Poria, and E. Cambria, “Recent trends in deep learning based natural language processing,” *IEEE Computational Intelligence Magazine*, vol. 13, no. 3, pp. 55–75, 2018.
9. I. J. Goodfellow, J. Shlens, and C. Szegedy, “Explaining and harnessing adversarial examples,” in *Inter. Conf. on Learning Representations*, 2015.
10. N. Papernot, P. McDaniel, S. Jha, M. Fredrikson, Z. B. Celik, and A. Swami, “The limitations of deep learning in adversarial settings,” in *IEEE European Symp. on Security and Privacy*. IEEE, 2016, pp. 372–387.
11. N. Carlini and D. Wagner, “Towards evaluating the robustness of neural networks,” in *IEEE Symp. on Security and Privacy*. IEEE, 2017, pp. 39–57.

12. A. Madry, A. Makelov, L. Schmidt, D. Tsipras, and A. Vladu, "Towards deep learning models resistant to adversarial attacks," *arXiv preprint arXiv:1706.06083*, 2017.
13. C. Xiao, B. Li, J. Zhu, W. He, M. Liu, and D. Song, "Generating adversarial examples with adversarial networks," *arXiv preprint arXiv:1801.02610*, 2018.
14. C. Xiao, J. Zhu, B. Li, W. He, M. Liu, and D. Song, "Spatially transformed adversarial examples," *arXiv preprint arXiv:1801.02612*, 2018.
15. N. Papernot, P. McDaniel, and I. Goodfellow, "Transferability in machine learning: from phenomena to black-box attacks using adversarial samples," *arXiv preprint arXiv:1605.07277*, 2016.
16. Y. Liu, X. Chen, C. Liu, and D. Song, "Delving into transferable adversarial examples and black-box attacks," *arXiv preprint arXiv:1611.02770*, 2016.
17. N. Inkawhich, K. J. Liang, L. Carin, and Y. Chen, "Transferable perturbations of deep feature distributions," *arXiv preprint arXiv:2004.12519*, 2020.
18. A. Ilyas, S. Santurkar, D. Tsipras, L. Engstrom, B. Tran, and A. Madry, "Adversarial examples are not bugs, they are features," *Advances in Neural Information Processing Systems*, vol. 32, 2019.
19. A. I. Maqueda, A. Loquercio, G. Gallego, N. García, and D. Scaramuzza, "Event-based vision meets deep learning on steering prediction for self-driving cars," in *Proc. of the IEEE Conf. on Computer Vision and Pattern Recognition*, 2018, pp. 5419–5427.
20. M. Bojarski, D. Del Testa, D. Dworakowski, B. Firner, B. Flepp, P. Goyal, L. D. Jackel, M. Monfort, U. Muller, J. Zhang *et al.*, "End to end learning for self-driving cars," *arXiv preprint arXiv:1604.07316*, 2016.
21. S. Kariyappa and M. K. Qureshi, "Improving adversarial robustness of ensembles with diversity training," *arXiv preprint arXiv:1901.09981*, 2019.
22. T. Pang, K. Xu, C. Du, N. Chen, and J. Zhu, "Improving adversarial robustness via promoting ensemble diversity," in *Inter. Conf. on Machine Learning*. PMLR, 2019, pp. 4970–4979.
23. S. Sen, B. Ravindran, and A. Raghunathan, "EMPIR: Ensembles of mixed precision deep networks for increased robustness against adversarial attacks," in *Inter. Conf. on Learning Representation*, 2020, pp. 1–12.
24. S. Zhang, M. Liu, and J. Yan, "The diversified ensemble neural network," *Advances in Neural Information Processing Systems*, vol. 33, pp. 16 001–16 011, 2020.
25. Z. Yang, L. Li, X. Xu, S. Zuo, Q. Chen, P. Zhou, B. Rubinstein, C. Zhang, and B. Li, "TRS: Transferability reduced ensemble via promoting gradient diversity and model smoothness," *Advances in Neural Information Processing Systems*, vol. 34, 2021.
26. B. Guo, S. Han, X. Han, H. Huang, and T. Lu, "Label confusion learning to enhance text classification models," in *Proc. of the AAAI Conf. on Artificial Intelligence*, 2020.
27. K. Ren, T. Zheng, Z. Qin, and X. Liu, "Adversarial attacks and defenses in deep learning," *Engineering*, vol. 6, no. 3, pp. 346–360, 2020.
28. X. Yuan, P. He, Q. Zhu, and X. Li, "Adversarial examples: Attacks and defenses for deep learning," *IEEE Transactions on Neural Networks and Learning Systems*, vol. 30, no. 9, pp. 2805–2824, 2019.
29. H. Xu, Y. Ma, H.-C. Liu, D. Deb, H. Liu, J.-L. Tang, and A. K. Jain, "Adversarial attacks and defenses in images, graphs and text: A review," *International Journal of Automation and Computing*, vol. 17, no. 2, pp. 151–178, 2020.
30. A. Kurakin, I. Goodfellow, S. Bengio *et al.*, "Adversarial examples in the physical world," 2016.

31. Y. Dong, F. Liao, T. Pang, H. Su, J. Zhu, X. Hu, and J. Li, “Boosting adversarial attacks with momentum,” in *Proceedings of the IEEE conference on computer vision and pattern recognition*, 2018, pp. 9185–9193.
32. Z. Akata, F. Perronnin, Z. Harchaoui, and C. Schmid, “Label-embedding for image classification,” *IEEE Transactions on Pattern Analysis and Machine Intelligence*, vol. 38, no. 7, pp. 1425–1438, 2016.
33. R. Muller, S. Kornblith, and G. E. Hinton, “When does label smoothing help,” *arXiv: Learning*, 2019.
34. X. Zhang, Q.-W. Zhang, Z. Yan, R. Liu, and Y. Cao, “Enhancing label correlation feedback in multi-label text classification via multi-task learning,” *arXiv preprint arXiv:2106.03103*, 2021.
35. C. Fu, H. Chen, N. Ruan, and W. Jia, “Label smoothing and adversarial robustness,” *arXiv preprint arXiv:2009.08233*, 2020.
36. Y. Wang, Y. Zheng, Y. Jiang, and M. Huang, “Diversifying dialog generation via adaptive label smoothing,” *arXiv preprint arXiv:2105.14556*, 2021.
37. S. Kullback and R. A. Leibler, “On information and sufficiency,” *Annals of Mathematical Statistics*, vol. 22, no. 1, pp. 79–86, 1951.
38. M. Menéndez, J. A. Pardo, L. Pardo, and M. C. Pardo, “The jensen-shannon divergence,” *Journal of the Franklin Institute*, vol. 334, no. 2, pp. 307–318, 1997.
39. L. Deng, “The MNIST database of handwritten digit images for machine learning research,” *IEEE Signal Processing Magazine*, vol. 29, no. 6, pp. 141–142, 2012.
40. H. Xiao, K. Rasul, and R. Vollgraf, “Fashion-MNIST: a novel image dataset for benchmarking machine learning algorithms,” *arXiv preprint arXiv:1708.07747*, 2017.
41. A. Krizhevsky and G. Hinton, “Learning multiple layers of features from tiny images,” *Technical Report, Department of Computer Science, University of Toronto*, 2009.
42. D. P. Kingma and J. Ba, “Adam: A method for stochastic optimization,” *arXiv preprint arXiv:1412.6980*, 2014.
43. G. W. Ding, L. Wang, and X. Jin, “AdverTorch v0. 1: An adversarial robustness toolbox based on pytorch,” *arXiv preprint arXiv:1902.07623*, 2019.
44. H. Yang, J. Zhang, H. Dong, N. Inkawhich, A. Gardner, A. Touchet, W. Wilkes, H. Berry, and H. Li, “DVERGE: diversifying vulnerabilities for enhanced robust generation of ensembles,” *Advances in Neural Information Processing Systems*, vol. 33, pp. 5505–5515, 2020.
45. Y. LeCun, B. Boser, J. S. Denker, D. Henderson, R. E. Howard, W. Hubbard, and L. D. Jackel, “Backpropagation applied to handwritten zip code recognition,” *Neural Computation*, vol. 1, no. 4, pp. 541–551, 1989.